

Computational study of interstitial hydrogen atoms in nano-diamond grains embedded in an amorphous carbon shell

Amihai Silverman

Taub Computer Center, Technion-IIT, Haifa 32000, Israel

Alon Hoffman

Schulich Faculty of Chemistry, Technion-IIT, Haifa 32000, Israel

Joan Adler

Department of Physics, Technion-IIT, Haifa 32000, Israel

(Dated: December 16, 2008)

Abstract

The properties of hydrogen atoms in a nano-diamond grain surrounded by an amorphous carbon shell are studied with Tight Binding computer simulations. Our samples model nano-diamond grains, of a few nanometers in size, that nucleate within an amorphous carbon matrix, as observed in deposition from a hydrocarbon rich plasma. The calculations show that the average hydrogen interstitial formation energy in the amorphous region is lower than in the nano-diamond core. This formation energy difference is the driving force for the diffusion of hydrogen atoms from nano-diamond grains into amorphous carbon regions. An energy well was observed on the amorphous side of the nano-diamond amorphous carbon interface: atoms which diffuse from the diamond to the amorphous region are expected to be localized here. This scenario agrees with experimental results which show that hydrogen retention of diamond films increases with decreasing grain size, and suggest that hydrogen is bonded and trapped in nano-diamond grain boundaries and on internal grain surfaces.

I. INTRODUCTION

Hydrogen is an essential component of the gas mixture used for micro and nano crystalline diamond film nucleation and growth by Chemical Vapor Deposition (CVD) methods¹⁻³. Extensive research has been carried out to determine the role of hydrogen in this process. When such deposition is made with energetic species, hydrogen-rich carbon films with nano-diamond grains a few nanometers in size, embedded into an amorphous carbon matrix⁴, are created. The deposition parameters and properties of this class of films were extensively investigated and it was found that their formation is accompanied by a large hydrogen retention which was postulated to decorate the diamond grain boundaries⁵. It was recently reported by us and others that hydrogen retention in diamond films increases with decreasing diamond grain size⁶. In addition to the postulated location of hydrogen in the grain boundaries, other possible hydrogen locations are within the diamond grains as interstitial sites, forming defect-H clusters in the grains, on the diamond surfaces, or in non-diamond constituents between the grains (e.g. when nano-diamond crystallines are embedded in an a-C/graphite matrix).

In order to provide answers to key questions surrounding the location and properties of the hydrogen sites in diamond films, we carried out computer simulations with Tight Binding Molecular Dynamics (TBMD) methods. We calculated and compared the properties and energies of hydrogen atom interstitial sites in simulated samples of diamond, amorphous carbon and in mixed samples with an interface between a nano-diamond grain and an amorphous carbon shell. In a TBMD simulation, the band structure energy and the many body forces are calculated directly by diagonalizing the one electron Hamiltonian matrix^{7,8}. Since the method is less computationally intensive than Local Density Approximation (LDA)^{9,10} calculations, it allows us to study larger systems of atoms. Thus we can include important structural configurations such as nano-diamond in an amorphous matrix, and thereby study the interface region between diamond and amorphous structures.

Starting from translationally invariant pure diamond, our calculations were carried out in two stages. First, preliminary samples were prepared, using simpler molecular dynamics methods with empirical potentials^{11,12}, because relatively long run times are sometimes needed at this stage. A melt-quench process^{13,14} was used to prepare either amorphous carbon, or a nano-diamond core surrounded by an amorphous carbon matrix. For the

latter, some diamond sites were pinned during the melt-quench process to imitate a nano-diamond grain embedded into an amorphous carbon matrix after the nucleation process which was observed in the experiment⁴. (Smaller samples with the inverse structures of amorphous cores and crystalline surroundings, were previously generated in our group with this approach¹⁵). Once the preliminary samples were obtained, a TBMD simulation using the Frauenheim's Tight Binding (FTB) model^{7,8} was applied for both the C-H and C-C interactions to stabilize the sample, and obtain more accurate atomic configurations. In all cases, the initial sample was translationally invariant pure diamond.

After the two stage preparation process was completed, hydrogen atoms were inserted into the sample interiors and optimization techniques using the FTB model^{7,8} were applied to calculate the atomic configuration at the local-minimum in energy. The same process was performed for a large number of samples of the three types (diamond, amorphous and mixed); in each case one hydrogen atom was placed at a different interstitial site. The calculated hydrogen interstitial formation energies were plotted versus the distance from the interface between the diamond and the amorphous carbon. A preliminary version of some of the hydrogen interstitial results was given in Ref. 16. For comparison purposes we also calculated the hydrogen atom formation energy in a pure diamond core for different hydrogen concentrations.

In the following sections we first describe the sample preparations in details, and then present the results of our simulations. Then, we discuss these results in the light of the experimental measurements of hydrogen retention in diamond films carried out at the Technion.

II. SIMULATION SAMPLES AND METHODS

Our samples consisted of 512 carbon atoms in a (100) cubic cell with periodic boundary conditions, and were initially in a pure diamond structure. Two different procedures were then used to prepare amorphous and mixed diamond/amorphous samples.

A. Amorphous carbon samples

The amorphous structures were obtained using a molecular dynamics melt-quench process^{13,14}. The Parrinello-Rahman¹⁷ NPT (fixed number of atoms N, pressure, P, and temperature T) ensemble molecular dynamics algorithm was applied to melt the sample with all atoms free to move. Then, the sample was gradually cooled to allow the convergence of its volume, until equilibrium was obtained. The Stillinger-Weber¹¹ type empirical inter-atomic potentials, improved by Barnard-Russo¹² for tetrahedral carbon were used for the molecular dynamics inter-atomic force calculations at this initial melt-quench stage. Although such empirical inter-atomic potentials are less accurate than Tight Binding and Local Density Approximation (LDA)^{9,10}, and can not access quantum mechanical phenomena such as bond breaking and recombination, they can successfully simulate the formation of an amorphous structure using a melt-quench process¹³. In fact they are the practical choice for the formation stage since other methods are too slow for simulating the long amorphous samples formation process for large samples with the required degree of equilibration. Careful annealing, with equilibrium at each temperature is essential for the development of stable amorphous structures in carbon¹⁸.

At the end of the initial formation process, an additional, relatively long, molecular dynamics simulation using the Frauenheim's Tight Binding (FTB) model^{7,8} was applied to stabilize the sample, into even more accurate atomic configurations. These calculations used the PLATO code^{19,20}; with Conjugate Gradient (CG) algorithms²¹ using the FTB model applied to obtain the final atomic configuration.

B. Mixed diamond/amorphous

The mixed samples consist of a nano-diamond core surrounded by a region of amorphous carbon. These samples were also obtained by a simulation of a melt-quench process^{13,14} of initial samples with a pure diamond structure, but 150 atoms in the core of the samples were pinned (i.e. not allowed to move) during the simulations¹⁵. After initial equilibration the same Parrinello-Rahman¹⁷ NPT molecular dynamics algorithm was applied to the other 362 atoms followed again by a long molecular dynamics simulation using the FTB model to stabilize the sample.

C. Hydrogen interstitial sites

In the next stage, hydrogen atoms were inserted into interstitial sites of the three different sample types - diamond, amorphous and mixed. Four different amorphous samples and four different mixed samples were obtained by a melt-quench process using different time and temperature intervals during the formation process. Then, hydrogen atoms were inserted into random locations in the samples, and Conjugate Gradient (CG) and Steepest Descent (SD) optimization methods²¹ were used alternatively for the convergence of the atomic coordinates toward the local-minimum in energy using the FTB models^{7,8}. At this stage all the atoms were allowed to move, and at the end all the hydrogen atoms were located in interstitial sites. The mixed samples had only one hydrogen atom inserted, but multiple hydrogen atoms were inserted into the pure diamond sample and the amorphous samples for comparison purposes. The process of hydrogen interstitial site calculation was repeated roughly 100 times for different sites in the mixed samples, and roughly 30 times for different sites in the amorphous samples.

D. Visualization

The atomic images in this article were drawn using AViz²², and different greyscale values (color online) were used to indicate different atomic types.

III. SIMULATED SAMPLES - CHARACTERISTICS AND COMPARISON WITH NEXAFS

A. NEXAFS compared to DOS calculations

The Near Edge X-ray Absorption Fine Structure (NEXAFS)²³ can be simulated from the electronic structure as calculated from computer simulations such as tight binding. Some initial steps towards such comparisons were made previously²⁴ and are developed more fully below. We find that these comparisons provide a powerful validation of the characteristics of our simulated samples, and together with comparisons with the Density of States (DOS) and Radial Distribution Functions (RDF) calculated by other groups²⁵⁻²⁷ justify the physical basis of our computer simulation processes implemented for the generation of the amorphous

carbon and mixed samples.

The NEXAFS spectrum near the core level excitation edge may be described to a first approximation by a summation over all optical transitions between the C(1s) and the unoccupied electronic states. Therefore it is expected that the NEXAFS intensity at each point in the energy scale will depend on the specific geometry determined by the sample surface crystallographic orientation, incident photon source and detector orientation. However, the NEXAFS spectrum of amorphous carbon is not expected to display this dependency since the selection rules “soften” or even break down the optical modes that are normally forbidden in the spectra of crystalline samples. These modes are therefore activated and contribute to the NEXAFS spectrum. Therefore a comparison between the NEXAFS and DOS near the excitation edge is justified for amorphous carbon, and one would expect both curves to display features at similar energies (with respect to the Fermi level) as was observed. More details on the comparisons for the amorphous situation are given below.

B. Pure diamond

For the case of pure diamond the DOS/NEXAFS comparison may be less justifiable a priori since optical transition selection rules may have an important effect on the NEXAFS spectrum. Nevertheless, keeping this in mind, a general qualitative comparison may be made between the calculated DOS and the NEXAFS of diamond²³.

Our calculation for the DOS of our initial pure diamond sample, made with the FTB model⁷, was compared with the NEXAFS of a pure diamond sample measured by us²⁸. The NEXAFS measurements were carried out in the Partial Electron Yield (PEY) mode at SuperAco France using photon energies in the 285 - 320 eV range²⁸. Figure 1 shows the calculation of the DOS of a pure diamond sample above the Fermi level versus NEXAFS experimental results for a pure diamond sample. The NEXAFS plot was shifted along the X (energy) axis so that the first positive yield coincides with the Fermi level of the DOS calculation. From this figure a relatively good qualitative correspondence is observed between the features in the DOS and NEXAFS spectrum. An exception is the sharp NEXAFS peak measured at ~ 1 eV (full width at half maximum of 0.2 eV) which is associated with a bulk C(1s) exciton and therefore not expected to appear as a feature in the ground state DOS.

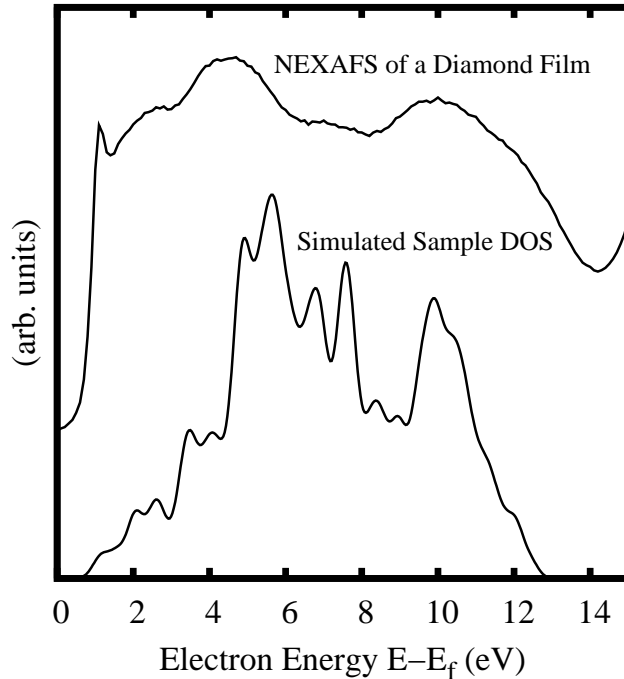


FIG. 1: A Pure diamond simulated sample Density of States (DOS) above the Fermi level (lower plot) versus NEXAFS experimental results for a pure diamond film (upper plot).

C. Amorphous Carbon

An image of one of our amorphous samples, obtained from a simulated melt-quench process, (see section II A) is presented in Figure 2 to aid the reader. Note that while the nearest neighbor distances are fairly similar, higher neighbor configurations and distances become quite irregular, and many atoms are three or two fold coordinated. Figure 3 depicts the calculated RDF, $g(r)$, of the amorphous sample, and figure 4 shows the electronic DOS of the amorphous sample which was calculated using the FTB model⁷. The RDF and DOS results of our amorphous carbon samples are in agreement with other simulated samples of amorphous carbon obtained using different models for the inter-atomic interactions²⁵⁻²⁷.

We compared the calculated DOS with the NEXAFS of an amorphous carbon film which were produced by in-situ 1000 eV Ar ion irradiation of a polycrystalline diamond film at a dose of $\sim 5 \times 10^{15}$ ions/cm²²⁸. Figure 5 shows the simulated amorphous sample DOS above the Fermi level, compared with the NEXAFS of an amorphous carbon film²⁸. The NEXAFS

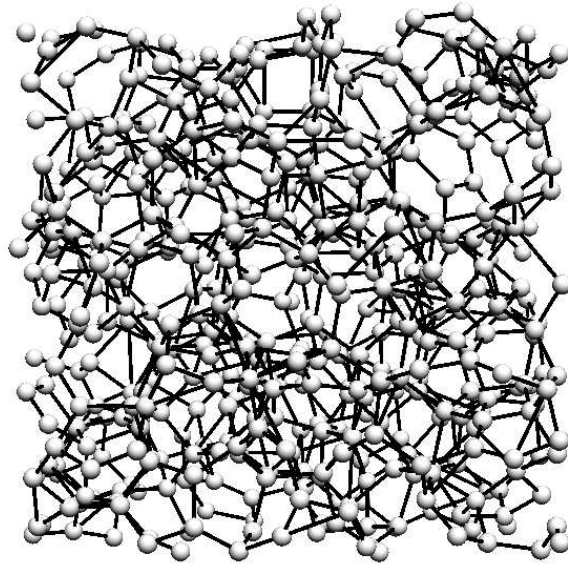


FIG. 2: A view of the amorphous carbon sample.

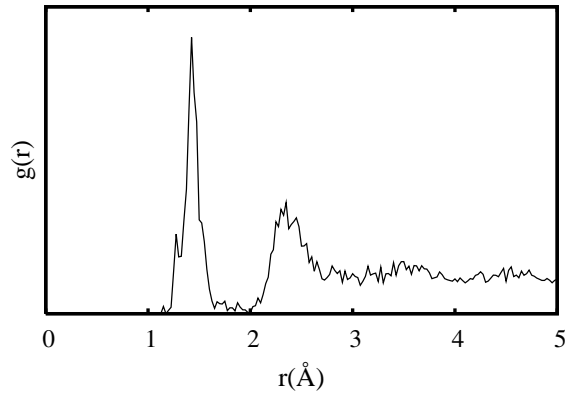


FIG. 3: Radial Distribution Function (RDF) of the amorphous carbon sample.

plot was shifted along the X (energy) axis so that the first positive yield coincides with the Fermi level of the DOS calculation.

As can be observed in figure 5, the calculated DOS above the Fermi level and the NEXAFS spectrum of the amorphous film display two peaks at very similar energies, 3 eV and 15 eV (with respect to the Fermi level). Considering that the NEXAFS spectrum in this energy range reflects the electronic DOS, the agreement between both spectra strongly confirm the validity of our amorphous carbon computational model.

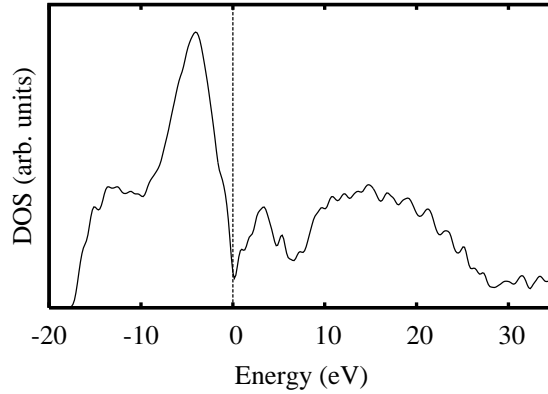


FIG. 4: Density of States (DOS) of the simulated amorphous carbon sample. The zero of the energy is taken to be the Fermi level (denoted by the vertical line).

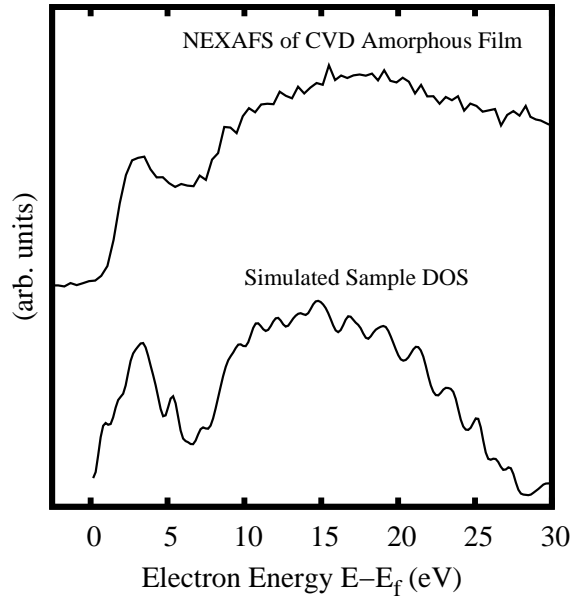


FIG. 5: The amorphous carbon simulated sample Density of States (DOS) above the Fermi level (lower plot) versus NEXAFS experiment results of a CVD amorphous carbon film (upper plot).

D. Mixed Sample

In order to understand nano-diamond film formation from energetic species⁴, simulated samples of a nano-diamond grain surrounded by an amorphous shell were prepared (see section II B). Figure 6 depicts an image of one of these mixed samples. Different time and

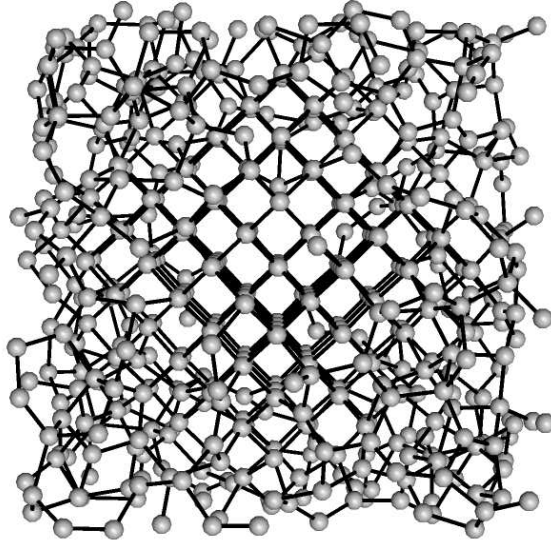


FIG. 6: A view of the mixed sample - a nano-diamond core surrounded by amorphous carbon shell.

temperature steps were used to form a number of different samples. The Radial Distribution Function (RDF) calculated for the 362 shell atoms (not shown here, but similar to figure 3) revealed the characteristic pattern of an amorphous structure¹⁴, confirming the amorphous nature of the shell atoms.

IV. HYDROGEN INTERSTITIAL SITES

In the following sections, we describe the behavior of our pure diamond, amorphous carbon and mixed samples when hydrogen atoms were inserted into interstitial sites.

A. Hydrogen interstitial sites in pure diamond

The structure and energy of hydrogen interstitial sites in pure diamond samples were calculated. This was carried out by inserting hydrogen atoms into random locations inside pure diamond samples, and relaxing the atomic configurations into the energy minimum. Two interstitial sites were observed, Bond-Centered (BC) and Tetrahedral (T) (in agreement with others²⁹⁻³¹). We found for the BC and T sites interstitial formation energies of $E_{H_{BC}}(i) = 3.72eV$ and $E_{H_T}(i) = 5.30eV$ respectively, where the C-H bond lengths are $l_{H_{BC}}(i) = 1.186\text{\AA}$ and $l_{H_T}(i) = 1.632\text{\AA}$.

The addition of a single hydrogen interstitial into pure diamond means a defect is formed

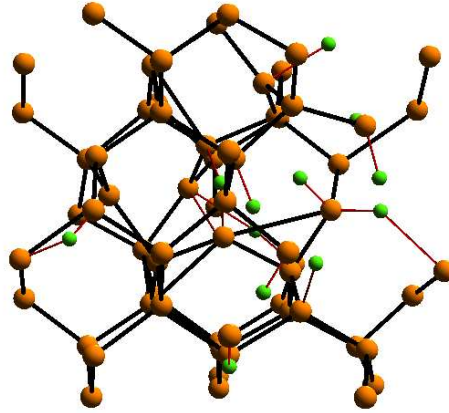


FIG. 7: (Color online) A view of a portion of an initial pure diamond after 20 at.% hydrogen atoms were inserted. The large circles (orange online) depict carbon atoms and the small spheres (green online) depict hydrogen atoms.

and therefore the system energy is increased. For example, at a BC site, the hydrogen atom inserts itself into a C-C bond resulting in a stretched C-C bond. Adding another hydrogen interstitial near the one already present forms an Anti-Bonding (AB) site, which results in a decrease in the binding energy per hydrogen atom, thereby decreasing the interstitial formation energy per atom³².

We observed that when further hydrogen atoms were added into pure diamond and the density was allowed to relax, the hydrogen interstitial formation energy was reduced significantly (i) as the hydrogen concentration increased, and (ii) as the sample density decreased. These effects are additive as increasing the hydrogen concentration increases the sample volume, and therefore reduces the density of the carbon atoms.

In order to check this systematically, a number of hydrogen atoms were gradually inserted into random sites in an initially pure diamond sample, and the energy was calculated after relaxation. After each insertion the Steepest Descent (SD) optimization method²¹ was used to map the atomic configuration into the minimum energy configuration, then the density of the sample was mapped to the minimum energy density, and the energy of the sample E_{H_n} was calculated. All the energies were calculated using the FTB model⁷ with periodic boundary conditions. A view of a portion of a sample with several hydrogens inserted is shown in Figure 7.

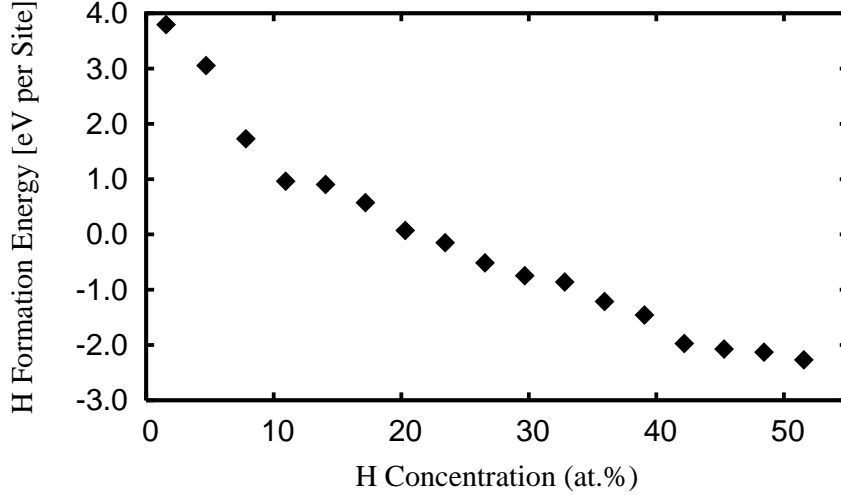


FIG. 8: The average hydrogen interstitial formation energy in an initial pure diamond with hydrogen interstitial sites, as a function of hydrogen concentration.

In figure 8 the hydrogen interstitial formation energy per hydrogen atom $E_{H_n}(i)$ is plotted as a function of the hydrogen concentration, where $E_{H_n}(i) = \frac{E_{H_n} - E_x - E_H(\text{vac})}{n}$. E_{H_n} is the energy of the sample with n hydrogen atoms at interstitial sites, E_x is the energy of the initial pure diamond sample, and $E_H(\text{vac}) = -5.44\text{eV}$ is the FTB energy of a hydrogen atom in vacuum.

We observe that the average hydrogen interstitial formation energy decreases with increasing hydrogen concentration. This behavior is explained as follows: after inserting hydrogen atoms into a pure diamond sample, the volume is increased and defects and dangling bonds are formed. When more hydrogen atoms are inserted, they enter into defect sites, terminate dangling bonds and therefore reduce the system energy. The higher the hydrogen concentration, the more defects are formed.

From Figure 8 we also observe that the hydrogen interstitial formation energy is positive when the hydrogen concentration is below 20 at.%, and negative elsewhere. Therefore, inserting a low concentration of hydrogen into a pure diamond increases the system energy, but once the hydrogen concentration rises above some 20 at.%, inserting additional hydrogen atoms decreases the system energy.

B. Hydrogen interstitial sites in amorphous carbon

Different interstitial site locations for hydrogen were examined for different simulated amorphous carbon samples, and the hydrogen interstitial formation energies $E_H(i)$ for different hydrogen interstitials were calculated as $E_H(i) = E_H - E_x - E_H(\text{vac})$ where E_H is the energy of the sample with a hydrogen atom at an interstitial site, E_x is the energy of the initial amorphous carbon sample (without the hydrogen atom) and $E_H(\text{vac})$ is the energy of a hydrogen atom in vacuum (all energies were calculated using the FTB model⁷). On averaging $E_H(i)$ over different amorphous carbon samples and different hydrogen sites we found $E_H(i)_{\text{av}} = -5.2 \pm 1.5\text{eV}$. The FTB model C-H bond energy is $E_{C-H} = -5.48\text{eV}$, within the range of $E_H(i)_{\text{av}}$, therefore we deduce that hydrogen atoms which were inserted into the amorphous carbon matrix were bonded to carbon atoms, terminating dangling bonds. Dangling bonds are widespread in amorphous carbon due to the disordered nature of the system where many carbon atoms are three-fold coordinated^{33,34}.

We also calculated the interstitial hydrogen formation energy in amorphous carbon samples with different hydrogen concentrations. The average hydrogen interstitial formation energies (averaged over different samples and different sites) fell within the same range for different hydrogen concentrations. Unlike the situation in pure diamond where the hydrogen interstitial sites form defects and therefore the energy per hydrogen interstitial site decreases with hydrogen concentration, in amorphous carbon, the hydrogen atoms do not create new defects, but are bonded to dangling bonds in existing defects, and therefore the energy per hydrogen interstitial site remains within the same range as the hydrogen concentration increases^{33,34}.

C. Hydrogen Interstitial sites in the Mixed Samples

Next, we inserted single hydrogen atoms into different interstitial sites of the mixed samples. The crystalline core of the sample has an almost spherical shape with radial symmetry (see figure 6), and therefore the interface between the crystalline core atoms and the amorphous layer is at the same radial distance from the center of the sample. The radial distance of each interstitial site from the center of the sample was calculated, and plotted versus the interstitial site energy. The hydrogen interstitial site energy was calculated in the

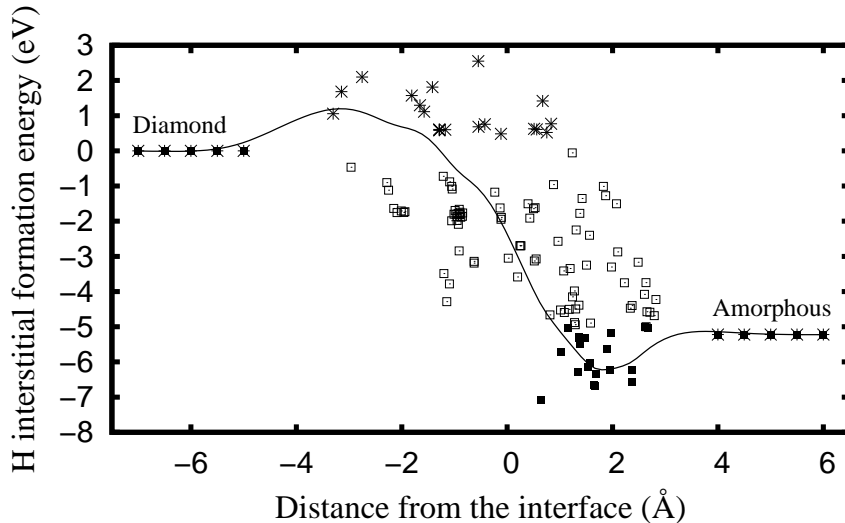


FIG. 9: The hydrogen interstitial formation energy $E_H(i)$ for different radial distances from the interface between the crystalline and amorphous regions. Each point represents a different hydrogen interstitial site. The asterisks represent hydrogen sites with positive energy, the squares represent hydrogen sites which decrease the system energy, and the filled squares represent the cases where the interstitial energy is lower than the interstitial energy in the amorphous carbon region. The continuous line depicts a cubic spline interpolation.

same way as in the previous section from $E_H(i) = E_H - E_x - E_H(\text{vac})$ except that here E_H is the energy of the mixed sample with the hydrogen atom in an interstitial site, E_x is the energy of the initial mixed sample without the hydrogen atom and $E_H(\text{vac})$ is the energy of a hydrogen atom in vacuum (calculated using the FTB model⁷).

In figure 9 the hydrogen interstitial energy $E_H(i)$ is plotted for various interstitial sites. The X axis is the radial distance of the hydrogen atom interstitial from the interface between the crystalline and amorphous regions, with the interface at $X = 0$. Each point in the plot represents a different interstitial site. The five points on the left-hand-side of the plot represent the average hydrogen site formation energy in pure diamond, as reported in section IV A (figure 8) for hydrogen concentration of 19 at.%. This concentration is that measured by us in nano-diamond films⁵. The five points on the right-hand-side represent the average hydrogen site formation energy in amorphous carbon (see section IV B).

Three different cases of interstitials were catalogued in the interface region. (i) Sites with

positive energy where the hydrogen atom creates a defect in the structure (similar to the case of hydrogen sites in pure diamond), and therefore increases the systems energy. (ii) Sites in the interface which decrease the system energy, obtained by terminating carbon dangling bonds. (iii) Sites where in addition to the termination of dangling bonds, the existence of a hydrogen site causes a structural relaxation of the neighboring carbon atoms, and therefore the total system energy is lower than the dangling bond termination energy. Since the structural change between the ordered nano-diamond and disordered amorphous carbon in the interface causes a strain which increases the system energy, some of the hydrogen interstitial sites in the interface relax this strain and therefore reduce the system energy. A cubic spline interpolation calculation²¹ has been made to interpolate between our data point.

We observe that in the diamond side of the interface region, there is a higher probability of finding sites with positive formation energy, where on the amorphous carbon side there are many sites with a negative formation energy, which is lower than the hydrogen formation energy in amorphous carbon.

V. SUMMARY AND CONCLUSIONS

We deduce that

- The average hydrogen interstitial formation energy in the amorphous region is lower than the hydrogen interstitial formation energy in the nano-diamond. This difference increases when the hydrogen concentration in the nano-diamond core decreases. The formation energy difference is a driving force for diffusion of hydrogen atoms from the nano-diamond core, toward the amorphous region.
- There are several different types of sites in the interface between the amorphous carbon and the nano-diamond core, sites where the hydrogen atoms are not bonded and therefore have a positive formation energy, and sites where the hydrogen atoms terminate carbon dangling bonds and therefore have negative formation energies.
- The sites with a positive formation energy are on the nano-diamond core side of the interface, and may form a barrier for the diffusion of hydrogen atoms from the nano-diamond core to the amorphous region. The barrier height decreases with decreasing

hydrogen concentration in the nano-diamond core.

- An energy well resulting from the high concentration of interstitial sites with a formation energy lower than the hydrogen interstitial formation energy in amorphous carbon is located at the amorphous layer side of the interface. Hydrogen atoms which diffuse from the nano-diamond core toward the amorphous region are expected to be trapped in this well, and therefore reduce the structural strain of the interface. This conclusion is in agreement with our experimental results which show that hydrogen retention of diamond films increases with decreasing grain size, indicating the likelihood that hydrogen is bonded and trapped in nano-diamond grain boundaries as well as on internal grain surfaces⁶.

Our simulations suggest that hydrogen is expected to diffuse from the nano-diamond region into the amorphous region and decorate the boundaries between a nano-diamond core and its surrounding amorphous shell. Invoking the eminently reasonable assumption that the amorphous shell models nano-diamond grain boundaries, our computational studies support our recent experimental results and conclusions.

Acknowledgments

The calculations were carried out on the Computational Physics Group computers at the Technion. We thank Eduardo Warszawski for helpful discussions.

-
- ¹ S. Michaelson, O. Ternyak, A. Hoffman, and Y. Lifshitz, *Appl. Phys. Lett.* **90**, 031914 (2007).
 - ² S. Michaelson, O. Ternyak, R. Akhvlediani, O. A. Williams, D. Gruen, and A. Hoffman, *Phys. Stat. Sol. (a)* **204**, 2860 (2007).
 - ³ S. Michaelson, O. Ternyak, R. Akhvlediani, A. Hoffman, A. Lafosse, R. Azria, O. A. Williams, and D. M. Gruen, *J. Appl. Phys.* **102**, 113516 (2007).
 - ⁴ Y. Lifshitz, X. Meng, S. Lee, R. Akhvlediani, and A. Hoffman, *Phys. Rev. Lett* **93**, 056101 (2004).
 - ⁵ A. Hoffman, A. Heiman, R. Akhveldiany, E. Lakin, E. Zolotoyabko, and C. Cytermann, *J. Appl. Phys.* **94**, 4589 (2003).

- ⁶ S. Michaelson, O. Ternyak, A. Hoffman, and Y. Lifshitz, *Appl. Phys. Letters* **90**, 031914 (2007).
- ⁷ T. Frauenheim, F. Weich, T. Köhler, S. Uhlmann, D. Porezag, and G. Seifert, *Phys. Rev. B* **52**, 11492 (1995).
- ⁸ M. Elstner, D. Porezag, G. Jungnickel, T. F. J. Elsner, S. Suhai, and G. Seifert, *Phys. Rev. B* **58**, 7260 (1998).
- ⁹ W. Kohn and L. J. Sham, *Phys. Rev* **140**, A1133 (1965).
- ¹⁰ R. Car and M. Parrinello, *Phys. Rev. Lett.* **55**, 2471 (1985).
- ¹¹ F. H. Stillinger and T. A. Weber, *Phys. Rev. B* **31**, 5262 (1985).
- ¹² A. Barnard and S. Russo, *Mol. Phys.* **100**, 1517 (2002).
- ¹³ A. Silverman, J. Adler, and R. Weil, *Thin Solid Films* **193/194**, 571 (1990).
- ¹⁴ R. Zallen, *The physics of amorphous solids* (Wiley-Interscience, New York, 1983).
- ¹⁵ A. Sorkin, J. Adler, and R. Kalish, *Phys. Rev. B* **70**, 064110 (2004).
- ¹⁶ S. Michaelson, R. Akhvediani, A. Hoffman, A. Silverman, and J. Adler, *Phys. Stat. Sol. (a)* **205**, 2099 (2008).
- ¹⁷ M. Parrinello and A. Rahman, *J. Appl. Phys.* **52**, 7158 (1981).
- ¹⁸ D. Saada, J. Adler, and R. Kalish, *Phys. Rev. B* **59**, 6650 (1999).
- ¹⁹ A. P. Horsfield, *Phys. Rev. B* **56**, 6594 (1997), efficient ab initio tight binding.
- ²⁰ A. P. Horsfield and A. M. Bratkovsky, *J. Phys. Condens. Mat.* **12**, R1 (2000).
- ²¹ W. H. Press, S. A. Teukolsky, W. T. Vetterling, and B. P. Flannery, *Numerical Recipes, The Art of Scientific Computing* (Cambridge University Press, 2007), 3rd ed.
- ²² J. Adler, R. K. J. Fox, T. Mutat, A. Sorkin, and E. Warszawski, *Computer Physics Communications* **177**, 19 (2007).
- ²³ J. Stöhr, *NEXAFS Spectroscopy (Springer Series in Surface Sciences)* (Springer, 2003).
- ²⁴ E. Warszawski, A. Hoffman, A. Silverman, and J. Adler, *Bulletin of the Israel Physical Society* **52**, 38 (2006).
- ²⁵ N. A. Marks, D. R. McKenzie, B. A. Pailthorpe, M. Bernasconi, and M. Parrinello, *Phys. Rev. B* **54**, 9703 (1996).
- ²⁶ N. A. Marks, D. R. McKenzie, B. A. Pailthorpe, M. Bernasconi, and M. Parrinello, *Phys. Rev. B* **54**, 9703 (1996).
- ²⁷ D. G. McCulloch, D. R. McKenzie, and C. M. Goringe, *Phys. Rev. B* **61**, 2349 (2000).
- ²⁸ A. Hoffman, M. Petracic, G. Comtet, A. Heurtel, L. Hellner, and G. Dujardin, *Phys. Rev. B*

- 59**, 3203 (1999).
- ²⁹ D. Saada, J. Adler, and R. Kalish, *Phys. Rev B* **61**, 10711 (2000).
- ³⁰ J. P. Goss, R. Jones, M. I. Heggie, C. P. Ewels, P. R. Briddon, and S. Oberg, *Phys. Stat. Sol. (a)* **186**, 263 (2001).
- ³¹ J. P. Goss, R. Jones, M. I. Heggie, C. P. Ewels, P. R. Briddon, and S. Oberg, *Phys. Rev. B* **65**, 115207 (2002).
- ³² S. Mehandru, A. B. Anderson, and J. Angus, *J. Mater. Res.* **7**, 689 (1992).
- ³³ N. M. J. Conway, A. Ilie, J. Robertson, W. I. Milne, and A. Tagliaferro, *Appl. Phys. Letters* **73**, 2456 (1998).
- ³⁴ A. von Keudell, M. Meier, and C. Hopf, *Diamond and Related Materials* **11**, 969 (2002).